

On Performance Loss of DOA Measurement Using Massive MIMO Receiver with Mixed-ADCs

Baihua Shi, Lingling Zhu, Wenlong Cai, Nuo Chen, Tong Shen, Pengcheng Zhu, Feng Shu, and Jiangzhou Wang, *Fellow, IEEE*

arXiv:2104.02447v1 [cs.IT] 6 Apr 2021

Abstract—High hardware cost and high power consumption of massive multiple-input and multiple output (MIMO) are still two challenges for the future wireless communications including beyond 5G. Adopting the low-resolution analog-to-digital converter (ADC) is viewed as a promising solution. Additionally, the direction of arrival (DOA) estimation is an indispensable technology for beam alignment and tracking in massive MIMO systems. Thus, in this paper, the performance of DOA estimation for massive MIMO receive array with mixed-ADC structure is first investigated, where one part of radio frequency (RF) chains are connected with high-resolution ADCs and the remaining ones are connected with low-resolution ADCs. Moreover, the Cramér-Rao lower bound (CRLB) for this architecture is derived based on the additive quantization noise model approximation for the effect of low-resolution ADCs. Then, the root-MUSIC method is designed for such a receive structure. Eventually, a performance loss factor and the associated energy efficiency factor is defined for analysis in detail. Simulation results find that a mixed-ADC architecture can strike a good balance among RMSE performance, circuit cost and energy efficiency. More importantly, just 1-4 bits of low-resolution ADCs can achieve a satisfactory performance for DOA measurement.

Index Terms—massive MIMO, DOA estimation, mixed-ADC, CRLB

I. INTRODUCTION

Direction of arrival (DOA) estimation has attracted lots of attention since its birth. It has wide application prospects, such as wireless communications, radar, radio astronomy, sonar, navigation, tracking of various objects, and rescue and other emergency assistance devices [1]–[3]. In the massive multiple-input multiple-output (MIMO) systems, it is also a key technology for its integral role in many emerging applications, including unmanned aerial vehicle (UAV) communications [4], wireless communications via intelligent reflecting surface [5]–[7], directional modulation systems [8]–[11], secure and precise wireless transmission systems [12]–[14], internet of things (IoT) [15], and millimeterwave-based massive MIMO for beyond 5G and so on.

B. Shi, L. Zhu, N. Chen and T. Shen are with the School of Electronic and Optical Engineering, Nanjing University of Science and Technology, Nanjing 210094, China.

W. Cai is with the National Key Laboratory of Science and Technology on Aerospace Intelligence Control, Beijing Aerospace Automatic Control Institute, Beijing 100854, China. (e-mail: caiwenlon@buaa.edu.cn).

P. Zhu is with National Mobile Communications Research Laboratory, Southeast University, Nanjing, China. (emails: p.zhu@seu.edu.cn).

F. Shu is with the School of Information and Communication Engineering, Hainan University, Haikou 570228, China. and also with the School of Electronic and Optical Engineering, Nanjing University of Science and Technology, Nanjing 210094, China. (e-mail: shufeng0101@163.com).

J. Wang is with the School of Engineering and Digital Arts, University of Kent, Canterbury CT2 7NT, U.K. (e-mail: j.z.wang@kent.ac.uk).

It is well-known that there are two main categories in DOA estimation methods: subspace based methods and parametric methods. Estimation of signal parameters via rotational invariance technique (ESPRIT) and multiple signal classification (MUSIC) are two most famous subspace based methods [16], [17]. To avoid spectral search in MUSIC, the author in [18] proposed a MUSIC-based search-free method, called root-MUSIC. Then, several modified root-MUSIC methods were proposed to further reduce the complexity, like unitary root-MUSIC (U-root-MUSIC) [19] and real-valued root-MUSIC (RV-root-MUSIC) [20]. Recently, these methods have been extended to massive MIMO systems. Authors in [21] investigated the DOA estimation in 2-D massive MIMO without knowledge of number of paths, noise power, path gain correlations and ill-conditioned data statistics. And, in order to reduce the circuit cost and power consumption in massive MIMO, authors in [22] extended that to the hybrid massive MIMO and proposed a low complexity 2D discrete Fourier transform (DFT) based estimation method. Moreover, the theoretical bounds of the mean squared errors (MSEs) and the Cramér-Rao lower bounds (CRLBs) of the joint DOA and channel gain estimation were derived. Authors in [23] proposed three low-complexity and high-resolution methods in hybrid massive MIMO systems: two parametric methods and a root-MUSIC-based method. The CRLB of the hybrid massive MIMO receive array was also derived. Then, more and more attention was paid to the DOA estimation in hybrid massive MIMO systems. In [24], a new design of analog phase shifts was proposed to tackle the phase ambiguities. However, the RMSE of that method is far to achieve the CRLB. In order to avoid the high complexity operation of the eigenvalue decomposition in DOA estimation, authors in [25] integrated the deep learning technique into massive MIMO systems. Furthermore, a deep-learning-based method for a hybrid uniform circular array (UCA) was firstly proposed in [26]. In [27], authors considered the DOA estimation with low-resolution analog-to-digital converters (ADCs) and revealed that the MUSIC method can be applied in one-bit systems without modification. Then, the performance of DOA estimation for low-resolution ADC structure was investigated in [28].

Due to the high hardware cost and high power consumption, it is still hard to adopt massive MIMO with several hundreds or more of antennas widely in practical applications. Every antenna is connected with a ADC in a radio frequency (RF) chain. And, a high-resolution ADC will consume the most power in a RF chain. In addition, its hardware cost also exponentially increases with the number of quantization

bits [29]. Hence, replacing high-resolution ADCs by low-resolution ADCs in massive MIMO is a promising solution. And, that have attracted much attention. However, it is hard to analyse the performance of nonlinear signal. Authors in [30] showed that the additive quantization noise model (AQNM) can be applied to eliminate that distortion caused by low-resolution ADCs. Based on this model, the closed-form expression of achievable rate was derived for multi-user (MU) massive MIMO systems with low-resolution ADCs in [31]. A multi-pair massive MIMO relay network was considered in [32]. Furthermore, instead of the asymptotic analysis, ergodic rates with finite number of antennas were derived. In [33], the achievable rate was derived for the multi-pair massive MIMO full-duplex relay system with low-resolution ADCs at both the relay station (RS) and destinations. In [34], authors investigated a multiuser massive MIMO amplify-and-forward relay uplink, where low-resolution ADCs are used at the RS. In [35], a two layer alternatively iterative scheme (TLAIS) was proposed in massive MIMO systems. And, authors successfully integrated low-resolution ADCs, finite-quantized phase shifters and hybrid structure into a massive MIMO system.

However, massive MIMO systems with pure low-resolution ADCs/DACs still face some tricky challenges, such as time-frequency synchronization, channel estimation, and achievable rate [36]–[38]. Thus, a new structure, mixed-ADC structure, was proposed in [39] to make up the shortcomings in low-resolution structure. In addition, the achievable data rates of the proposed system architecture was derived. Furthermore, The analysis was extended to ergodic fading channels. In this structure, some RF chains are connected with low-resolution ADCs/DACs and others with the high-resolution ADCs/DACs. Recently, lots of works have focused on the mixed-ADC structure. Spectral efficiency of massive MIMO systems with mixed-ADCs was investigated in [36]. And, this work verified that mixed-ADC receiver has a comparable spectral efficiency (SE) performance and a much lower hardware cost. Then, a new framework of detectors on a massive MIMO uplink system was presented in [40], which is developed through probabilistic Bayesian inference. In addition, the performance of this system was also investigated. In [37], authors investigated the performance of mixed-ADC massive MIMO systems over the Rician fading channel, which is more general for the practical scenarios. And, both closed-form approximate expressions for achievable rate with perfect and imperfect channel state information (CSI) were derived. Furthermore, authors in [38] revealed that the achievable rate with 2-3 quantization bits can approach that with pure high-resolution ADCs/DACs in massive MIMO relaying systems. In addition, a low-complexity efficient power allocation scheme in mixed-ADC architecture was proposed for the considered system. However, the DOA estimation for a massive MIMO system with mixed-ADC is still an open challenging problem.

To the best of our knowledge, there is little literature concerning the performance analysis of DOA estimation and its corresponding DOA measurement methods in mixed-ADC massive MIMO systems. Therefore, the performance and the energy efficiency of DOA estimation with mixed-ADCs are made a completed investigation. Then, the root-MUSIC

method is redesigned to suit such a mixed-ADC structure. It is also shown that the mixed-ADC is valuable in practical application due to its satisfactory performance and very low energy consumption. Our main contributions are summarized as follows:

- 1) To model the effect of the nonlinear errors caused by the coarse quantization, the AQNM is adopted to establish the linear system model of the DOA estimation with mixed-ADCs in massive MIMO systems. Then, based on that model, we prove that root-MUSIC can be utilized without modification for the mixed-ADC structure. From simulation results, we can make a conclusion that the root-MUSIC is able to achieve the CRLB of mixed-ADC structure. Furthermore, the mixed-ADC architecture has the same performance in the low SNR region.
- 2) In order to assess the performance of the DOA estimation with mixed-ADCs, the expression of the CRLB for mixed-ADC structure is derived by statistic theory and matrix theory. In addition, by defining the performance loss factor, the specific performance loss can be calculated through theoretical computations. Our analysis demonstrates that the mixed-ADC structure can reduce tremendous circuit cost and energy consumption with a negligible performance loss. And, similar to the analysis in [27], the mixed-ADC structure has less performance loss in the relatively low SNR region.
- 3) Finally, we make an investigation on the power consumption of the mixed-ADC structure. In order to achieve the maximum energy efficiency (EE), the EE factor of DOA estimation with mixed-ADC is first proposed. And, by resorting to the energy consumption model in [38], the optimal number of quantization bits for different proportions of high-resolution ADCs is given. In addition, We quantify the tradeoff between the CRLB and power consumption for different proportions of high-resolution ADCs and quantization bits of low-resolution ADCs. Together with the analysis of performance loss, simulation results also find that mixed-ADC architecture can work better in the massive MIMO scenario and low-resolution ADCs with 1-4 bits in mixed-ADC structure is sufficient to achieve a trivial performance loss.

The remainder of the paper is arranged as follows. System model is introduced in Section II. In Section III, we consider the application of root-MUSIC method in mixed-ADC massive MIMO. In Section IV, the corresponding CRLB for mixed-ADC structure is derived and the performance loss factor is also defined to measure performance loss. In Section V, an energy efficiency factor is defined for mixed-ADC massive MIMO systems. Simulation results are presented in Section VI. Finally, we draw our conclusions in Section VII.

Notations: Throughout the paper, \mathbf{x} and \mathbf{X} in bold typeface are used to represent vectors and matrices, respectively, while scalars are presented in normal typeface, such as x . Signs $(\cdot)^T$, $(\cdot)^H$, $|\cdot|$ and $\|\cdot\|$ represent transpose, conjugate transpose, modulus and norm, respectively. \mathbf{I}_M denotes the $M \times M$ identity matrix, $\mathbf{0}_{a \times b}$ denotes the $a \times b$ matrix of all zeros.

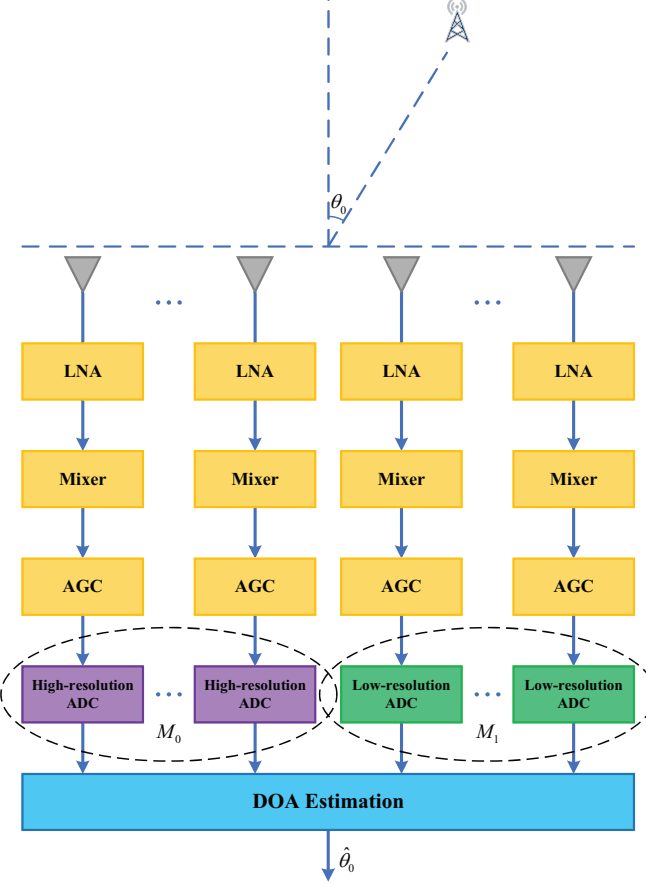


Fig. 1. System model of the mixed-ADC massive MIMO receive array with M_0 high-resolution ADCs and M_1 low-resolution ADCs.

Furthermore, $\mathbb{E}[\cdot]$ represents the expectation operator, and $\mathbf{x} \sim \mathcal{CN}(\mathbf{m}, \mathbf{R})$ denotes a circularly symmetric complex Gaussian stochastic vector with mean vector \mathbf{m} and covariance matrix \mathbf{R} . $\text{diag}(\mathbf{X})$ denotes a diagonal matrix by keeping only the diagonal elements of matrix \mathbf{X} . $\text{Tr}(\cdot)$ denotes matrix trace. \hat{x} represents the estimated value of x .

II. SYSTEM MODEL

As shown in Fig 1, we consider a uniform linear array (ULA) equipped with mixed-ADCs. This means that this array has M_0 high-resolution ADCs and M_1 low-resolution ADCs. The ULA has M antenna elements, and we define $\kappa \triangleq M_0/M (0 \leq \kappa \leq 1)$ as the proportion of high-resolution ADCs in the mixed-ADC architecture where $M = M_0 + M_1$. The narrow-band signal $s(t)e^{j2\pi f_c t}$ of a far-field emitter impinges on the array. Each antenna is composed of a low-noise amplifiers (LNA), a mixer, an automatic gain control (AGC) and an ADC. Note that LNA is able to amplify the receive signal, mixer is used to change the frequency of the received signal and the AGC is used to modify the amplitude of the received signal to use the full dynamic range of the ADC. Moreover, different received antennal elements will capture the signal at different time. Thus, the propagation delays of the m th antennal element is expressed by

$$\tau_m = \tau_0 - \frac{d_m}{c} \sin(\theta_0), \quad m = 1, 2, \dots, M, \quad (1)$$

where τ_0 is the propagation delay from the emitter to a reference point on the array, θ_0 is the direction of the emitter relative to the line perpendicular to the array, d_m , $m = 1, 2, \dots, M$ denote the distances of m th antennal element from the reference point and c denotes the speed of light. Thus, through RF chains, the signal is down-converted and the received signal vector can be written as

$$\mathbf{x}(t) = \mathbf{a}(\theta_0)s(t) + \mathbf{w}(t), \quad (2)$$

where $\mathbf{w}(t) \sim \mathcal{CN}(0, \mathbf{I}_M)$ is the additive white Gaussian noise (AWGN), $s(t)$ is the received signal and $\mathbf{a}(\theta_0)$ is the so-called array manifold, defined by

$$\mathbf{a}(\theta_0) = \left[e^{j2\pi\Psi_{\theta_0}(1)} \ e^{j2\pi\Psi_{\theta_0}(2)} \ \dots \ e^{j2\pi\Psi_{\theta_0}(M)} \right]^T, \quad (3)$$

where

$$\Psi_{\theta_0}(m) = \frac{d_m \sin \theta_0}{\lambda}, \quad m = 1, 2, \dots, M, \quad (4)$$

is the phase corresponding to the propagation delay of m th antennal element, where λ is the wavelength of the signal.

For the ease of expression and analysis, we denote the received signal as

$$\mathbf{x}(t) = \begin{bmatrix} \mathbf{x}_0(t) \\ \mathbf{x}_1(t) \end{bmatrix}, \quad (5)$$

where $\mathbf{x}_0(t)$, $\mathbf{x}_1(t)$ are the $M_0 \times 1$ and $M_1 \times 1$ vector, which denote the signals that will be quantized by high-resolution ADCs and low-resolution ADCs, respectively. Thus, the received signals experiencing the M_0 high-resolution ADCs can be written as

$$\mathbf{y}_0(n) = \mathbf{x}_0(t)|_{t=n} = \mathbf{a}_0(\theta_0)s(n) + \mathbf{w}_0(n), \quad n = 1, 2, \dots, N, \quad (6)$$

where N is the number of snapshots. Furthermore, we leverage on AQNM [34], [41], [42], which can approximate the non-linear quantization of the low-resolution ADCs as a linear gain with the additive quantization noise. Note that the AQNM model is precise when the SNR is middle and low. Then, the received signals are quantized each with a b -bit scalar quantizer and can be formulated as

$$\mathbf{y}_1(n) = \mathbb{Q}(\mathbf{x}_1(t)) \approx \alpha \mathbf{a}_1(\theta_0)s(n) + \alpha \mathbf{w}_1(n) + \mathbf{w}_q(n), \quad n = 1, 2, \dots, N, \quad (7)$$

where $\mathbf{w}_q(n)$ denotes the quantization noise, $\mathbb{Q}(\cdot)$ is the quantization function, and $\alpha = 1 - \beta$ is the linear quantization gain, where

$$\beta = \frac{\mathbb{E}[\|\mathbf{y} - \mathbf{y}_q\|^2]}{\mathbb{E}[\|\mathbf{y}\|^2]} \quad (8)$$

denotes the distortion factor of the low-resolution ADC. The accurate value of β is listed in Table I when $b \leq 5$. For longer quantization bitlength (e.g., $b > 5$), the distortion factor β can be approximated as

$$\beta \approx \frac{\sqrt{3}\pi}{2} \cdot 2^{-2b}, \quad b \geq 6. \quad (9)$$

TABLE I
DISTORTION FACTORS β FOR DIFFERENT ADCS QUANTIZATION BITS
($b \leq 5$)

b	1	2	3	4	5
β	0.3634	0.1175	0.03454	0.009497	0.002499

For a fixed channel realization, the covariance matrix of \mathbf{w}_q is given by

$$\begin{aligned}\mathbf{R}_w &= \alpha\beta\text{diag}(\sigma_s^2\mathbf{a}_1(\theta_0)\mathbf{a}_1^H(\theta_0) + \mathbf{I}_{M_1}) \\ &= \alpha\beta(\sigma_s^2 + 1)\mathbf{I}_{M_1}.\end{aligned}\quad (10)$$

From [41], \mathbf{w}_q can be modelled as $\mathbf{w}_q \sim \mathcal{CN}(0, \mathbf{R}_{w_F})$.

By combining (6) and (7), the overall received signal can be expressed as

$$\begin{aligned}\mathbf{y}(n) &= \begin{bmatrix} \mathbf{y}_0(n) \\ \mathbf{y}_1(n) \end{bmatrix} \\ &\approx \begin{bmatrix} \mathbf{a}_0(\theta_0)s(n) + \mathbf{w}_0(n) \\ \alpha\mathbf{a}_1(\theta_0)s(n) + \alpha\mathbf{w}_1(n) + \mathbf{w}_q(n) \end{bmatrix}.\end{aligned}\quad (11)$$

III. ANALYSIS FOR THE APPLICATION OF ROOT-MUSIC IN MIXED-ADC STRUCTURE

The Root-MUSIC proposed in [18] is a well-known subspace-based method for DOA estimation. By replacing the spectral search with finding roots of polynomials, it has a lower complexity without loss of performance. Thus, it is widely used in many scenes and has attracted much attention for many years. So, in this section, we extend the root-MUSIC algorithm to the mixed-ADC structure and prove the fact that there is no change on it.

When the array is equipped with pure high-resolution ADCs, the eigenvalue decomposition (EVD) of the covariance matrix \mathbf{R}'_y can be written as

$$\begin{aligned}\mathbf{R}'_y &= \mathbb{E}[\mathbf{y}\mathbf{y}^H] = \sigma_s^2\mathbf{a}\mathbf{a}^H + \mathbf{I}_M \\ &= \mathbf{E}_S\mathbf{\Lambda}_S\mathbf{E}_S^H + \mathbf{E}_W\mathbf{\Lambda}_W\mathbf{E}_W^H,\end{aligned}\quad (12)$$

where the columns of \mathbf{E}_S and \mathbf{E}_W are the eigenvectors corresponding to the useful signal and channel noise, respectively. Those can span the signal subspace and noise subspace, which are orthogonal. Thus, the spectrum,

$$S(\theta) = \|\mathbf{E}_W^H\mathbf{a}(\theta)\|^{-2},\quad (13)$$

will be infinity when $\theta = \theta_0$. To avoid a linear search, the root-MUSIC points out that we can solve the rooting polynomial with $2(M-1)$ degree as follow

$$f(z) = \mathbf{a}^T(z^{-1})\mathbf{E}_W\mathbf{E}_W^H\mathbf{a}(z),\quad (14)$$

where $\mathbf{a}(z) = [1, z^1, \dots, z^{M-1}]$. $f(z) = 0$ will have $2(M-1)$ roots and the largest root lying inside the unit circle is $z_0 = e^{j2\pi\frac{d\sin(\theta_0)}{\lambda}}$. Therefore, the estimated value can be given by

$$\hat{\theta}_0 = \arcsin\left(\frac{\lambda}{2\pi d}\arg z_0\right).\quad (15)$$

In practice, although the covariance matrix \mathbf{R}_y can not be obtained, that can be estimated from sampled data by

$$\hat{\mathbf{R}}_y = \frac{1}{N} \sum_{n=1}^N \mathbf{y}(n)\mathbf{y}^H(n).\quad (16)$$

In mixed-ADC structure, the covariance matrix \mathbf{R}_y can be casted as (17) at the bottom of this page, where $\gamma = \mathbb{E}[ss^H] = \sigma_s^2 = \sigma_s^2/\sigma_n^2$ is the input SNR of ADCs. Observing (17), $(\alpha^2 - 1)\gamma\mathbf{a}_1\mathbf{a}_1^H + (\gamma\alpha - 1)(1 - \alpha)\mathbf{I}_{M_1}$ and $\mathbf{a}_1\mathbf{a}_1^H$ have the identical eigenvectors. Thus, \mathbf{R}_ϵ can also be decomposed into one signal

$$\begin{aligned}\mathbf{R}_y &= \mathbb{E}[\mathbf{y}\mathbf{y}^H] = \begin{bmatrix} \gamma\mathbf{a}_0\mathbf{a}_0^H + \mathbf{I}_{M_0} & \gamma\alpha\mathbf{a}_0\mathbf{a}_1^H \\ \gamma\alpha\mathbf{a}_1\mathbf{a}_0^H & \gamma\alpha^2\mathbf{a}_1\mathbf{a}_1^H + \alpha^2\mathbf{I}_{M_1} + \mathbf{R}_w \end{bmatrix} \\ &= \gamma \underbrace{\begin{bmatrix} \mathbf{a}_0\mathbf{a}_0^H & \mathbf{a}_0\mathbf{a}_1^H \\ \mathbf{a}_1\mathbf{a}_0^H & \mathbf{a}_1\mathbf{a}_1^H \end{bmatrix}}_{\mathbf{R}'_y} + \mathbf{I}_M + \underbrace{\begin{bmatrix} \mathbf{0}_{M_0} & (\alpha - 1)\gamma\mathbf{a}_0\mathbf{a}_1^H \\ (\alpha - 1)\gamma\mathbf{a}_1\mathbf{a}_0^H & (\alpha^2 - 1)\gamma\mathbf{a}_1\mathbf{a}_1^H + (\gamma\alpha - 1)(1 - \alpha)\mathbf{I}_{M_1} \end{bmatrix}}_{\mathbf{R}_\epsilon}\end{aligned}\quad (17)$$

$$CRLB = \frac{3\lambda^2(\beta\gamma + 1)[\beta M_0(\gamma + 1) + \alpha M] + (\beta\gamma + 1)^2}{4K\pi^2\gamma\cos^2\theta_0 d^2[\beta M_0(\gamma + 1) + \alpha M][J_0(2M_0 - 1) + J(2M - 1)] - 3(J_0 + J)^2}\quad (20)$$

$$\begin{aligned}\eta_{PL} &= \frac{CRLB_{\kappa,\alpha}}{CRLB_{\kappa=1,\alpha=1}} = \frac{\gamma(g + \alpha)(g\kappa + \alpha) + \frac{(\beta\gamma + 1)^2}{M}}{\gamma + \frac{1}{M}} \\ &\cdot \frac{2\left(1 - \frac{1}{M}\right)\left(2 - \frac{1}{M}\right) - 3\left(1 - \frac{1}{M}\right)^2}{2(g\kappa + \alpha)\left[g\kappa\left(\kappa - \frac{1}{M}\right)\left(2\kappa - \frac{1}{M}\right) + \alpha\left(1 - \frac{1}{M}\right)\left(2 - \frac{1}{M}\right)\right] - 3\left[g\kappa\left(\kappa - \frac{1}{M}\right) + \alpha\left(1 - \frac{1}{M}\right)\right]^2}\end{aligned}\quad (25)$$

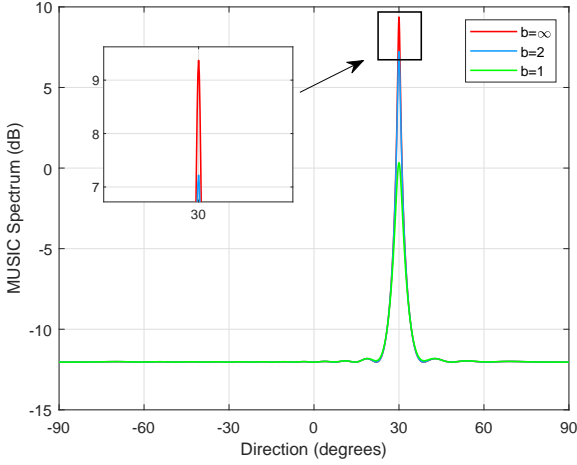


Fig. 2. MUSIC spectrum for a 32-element mixed-ADC ULA with an emitter at $\theta_0 = 30^\circ$, with $\gamma = 0\text{dB}$, $N = 128$, $\kappa = 1/2$, $b = 1, 2$ and ∞

eigenvalue and other noise eigenvalues, whose corresponding eigenvectors can span the approximate signal subspace and noise subspace with \mathbf{R}'_y . And, as the number of quantization bit increases, $\mathbf{R}_e \rightarrow \mathbf{0}_M$ and $\|\mathbf{R}_e\| \ll \|\mathbf{R}'_y\|$. Thus, $\mathbf{R}_y \approx \mathbf{R}'_y$ and \mathbf{R}_e can be considered as the error of \mathbf{R}'_y . Now, let \mathbf{e}' and λ' denote the eigenvalue and eigenvector of \mathbf{R}'_y , respectively. Then, we have

$$\mathbf{R}'_y \mathbf{e}' = \lambda' \mathbf{e}'. \quad (18)$$

Note that (18) can be regarded as the linear equations $\mathbf{R}'_y \mathbf{x} = \mathbf{b}$. And the condition number of \mathbf{R}'_y is given by

$$\text{cond}(\mathbf{R}'_y) = \frac{\|\lambda'_{\max}(\mathbf{R}'_y)\|}{\|\lambda'_{\min}(\mathbf{R}'_y)\|} = \gamma + 1. \quad (19)$$

Obviously, \mathbf{R}'_y has a low condition number. Thus, it is well-conditioned. And, we can conclude that \mathbf{R}'_y and \mathbf{R}_y will have the approximate eigenvalues and eigenvectors. As shown in Fig. 2, the MUSIC spectrum against the degree is presented. Although the peak of MUSIC spectrum for the ULA with mixed-ADC is lower than that of ULA with pure high-resolution ADCs, the directions are all at the correct DOA. And, the peak rises as the quantization bit of low-resolution ADCs increases. Therefore, the MUSIC method and root-MUSIC method can be applicable to the ULA with mixed-ADC structure without any modification.

IV. CRLB AND PERFORMANCE LOSS

The CRLB is the minimum variance of DOA estimation errors. It can provide a useful characterization of the achievable accuracy of the systems. In this section, to evaluate the performance of the massive MIMO for mixed-ADC architecture with different κ and b , the CRLB for the ULA with mixed-ADCs is derived in the appendix. Based on that, a new performance loss factor is defined to evaluate the accuracy loss of DOA estimation in mixed-ADC architecture.

Now, let us define $d_m = (m - 1)d$, according to Appendix, we have the CRLB for the ULA with mixed-ADC structure, (20), as shown at the bottom of this page, where

$$J_0 = \beta M_0(M_0 - 1)(\gamma + 1) \quad (21)$$

and

$$J = \alpha M(M - 1). \quad (22)$$

Moreover, when $\kappa = 1$ or $\alpha = 1$, which means that the ULA has none low-resolution ADC, the mixed-ADC architecture is going to degenerate into the conventional ULA equipped only with high-resolution ADCs. Note that if we choose the center of the array as the reference point, the corresponding CRLB will be identical to the derivation in [1], which is given by

$$\text{CRLB}_{\kappa=1, \alpha=1} = \frac{\lambda^2(\gamma M + 1)}{8K\pi^2\gamma^2 \cos^2 \theta_0 M \nu}. \quad (23)$$

Similarly, the CRLB of massive MIMO with low-resolution ADCs, $\kappa = 0$, can be given by

$$\text{CRLB}_{\kappa=0} = \frac{\lambda^2(\beta\gamma + 1)(\alpha\gamma M + \beta\gamma + 1)}{8\alpha^2 K \pi^2 \gamma^2 \cos^2 \theta_0 M \nu}. \quad (24)$$

Furthermore, let we define the performance loss factor η_{PL} by (25), where $g = \beta(\gamma + 1)$. And, that is shown at the bottom of this page. In massive MIMO systems, when the number of antenna elements grows without bound, $M \rightarrow \infty$, the η_{PL} will converge to

$$\eta_{PL} \approx \frac{(g + \alpha)(g\kappa + \alpha)}{4(g\kappa + \alpha)(g\kappa^3 + \alpha) - 3(g\kappa^2 + \alpha)^2}. \quad (26)$$

It is clear that, due to $0 \leq \kappa \leq 1$, η_{PL} is a linear monotonically increasing function of γ for a fixed κ and b . By contrary, η_{PL} decreases as κ and b increase. Details about which the quantization bit had better to be chosen are going to be discussed in Section VI.

V. ENERGY EFFICIENCY

Until now, we have analysed the performance loss and algorithm in mixed-ADC architecture. However, the performance will reach the peak definitely when ADCs are all high-resolution. Thus, to seek a basic trade-off between the performance and power consumption in the practical massive MIMO system, the energy efficiency of DOA estimation for mixed-ADC structure is discussed in this part.

To the best of our knowledge, no one has investigated the energy efficiency for DOA estimation with mixed-ADC structure. Thus, with the help of the definition in [43], we define the energy efficiency as

$$\eta_{EE} = \frac{\text{CRLB}^{-\frac{1}{2}}}{P_{total}} \text{ 1/degree/W}, \quad (27)$$

where P_{total} is the total power consumption in the massive MIMO system. $\text{CRLB}^{-1/2}$ represents the accuracy, which is the reciprocal of standard deviation lower bound and the unit of that is 1/degree. Referring to [44], P_{total} can be expressed as

$$\begin{aligned} P_{total} = & P_{syc} + M(P_{LNA} + P_{mix} + P_{fil} + P_{IFA}) \\ & + M_0(P_{AGC} + P_{ADC,H}) + M_1(cP_{AGC} + P_{ADC,L}) \end{aligned} \quad (28)$$

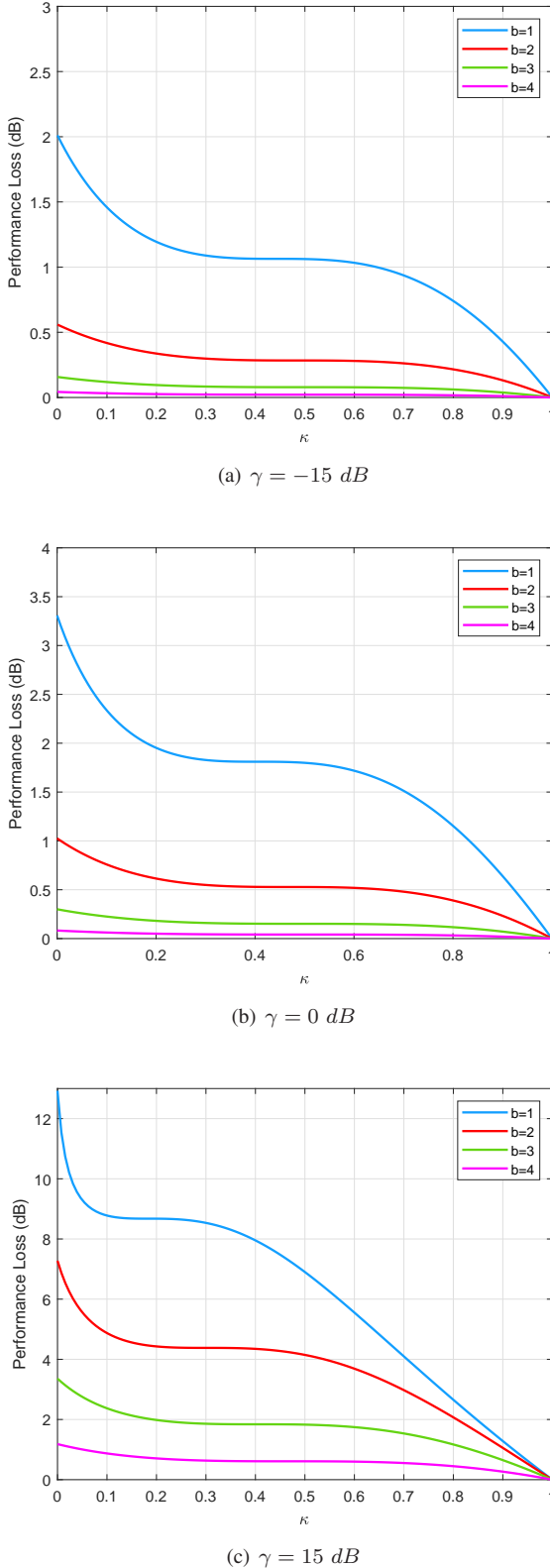


Fig. 3. Performance comparison of the DOA estimation over the κ with the different SNR and b .

where P_{syc} , P_{LNA} , P_{mix} , P_{fil} , P_{IFA} , P_{AGC} , P_{ADC_H} and P_{ADC_L} are the power consumption values for the frequency synthesizer, LNA, mixer, the active filters, the intermediate frequency amplifier (IFA), AGC, high-resolution ADCs, low-resolution ADCs, respectively. Besides, c is the flag function related to the quantization bits of the low-resolution ADCs, which is given by

$$c = \begin{cases} 0, & b = 1, \\ 1, & b > 1. \end{cases} \quad (29)$$

In accordance with [45], the power consumption values for ADCs can be calculated by

$$P_{ADC} \approx \frac{3V_{dd}^2 L_{min}(2B + f_{cor})}{10^{-0.1525b+4.838}}, \quad (30)$$

where B denotes the bandwidth of the signal, V_{dd} is the supply voltage of converter, L_{min} is the minimum channel length for the given CMOS technology, f_{cor} is the corner frequency of the $1/f$ noise [45]. (30) is established for the complete class of CMOS Nyquist-rate high speed ADCs [46].

VI. SIMULATION RESULTS AND DISCUSSIONS

In this section, we provide the theoretical performance simulation to analyse the effect of different proportions of high-resolution ADCs in the mixed-ADC architecture κ and quantization bits of low-resolution ADCs b on the performance loss η_{PL} . Furthermore, the simulation of root mean square error (RMSE) using root-MUSIC with different κ and b is conducted, where the RMSE is given by

$$RMSE = \sqrt{\frac{1}{N_t} \sum_{n_t=1}^{N_t} (\hat{\theta}_{n_t} - \theta_0)^2}. \quad (31)$$

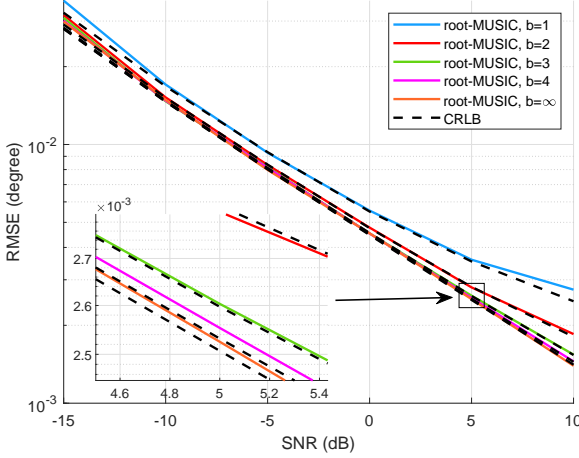
And, we consider the effect of SNR, the number of antennas and the number of snapshots on the root-MUSIC in the mixed-ADC architecture. In each simulation example, the number of estimation value N_t is 12000. In all simulations, we assume that an emitter is located in $\theta_0 = 30^\circ$, the number of snapshots K is 64 and the number of antenna elements M is 128 in the massive MIMO system.

In Fig. 3, curves of performance loss η_{PL} over the proportion of high-resolution ADCs κ with different b and SNR γ are illustrated respectively. We consider three different cases: $\gamma = -15 dB$, $\gamma = 0 dB$, $\gamma = 15 dB$. In each case, b ranges from 1 to 4. Obviously, we can see that η_{PL} is a monotonous decreasing function of κ . Furthermore, It can be seen that all curves are approximately flat between $\kappa = 0.2$ and $\kappa = 0.7$ but steep on both sides. Thus, κ can be divided into three ranges: $0 \sim 0.1$, $0.1 \sim 0.8$ and $0.8 \sim 1$. At low SNR, $\gamma = -15 dB$, the performance loss of 1-bit is far from being ignored at $\kappa < 0.1$. 2-bit low-resolution ADCs are more suitable, whose performance loss will be less than 1dB. As κ increases, 1-bit ADCs can be adopted with little performance loss. In addition, as the SNR increases, we should add the quantization bit to avoid considerable error. For example, $b = 2$ or $b = 3$ should be chosen at $\gamma < 0.1$ when $\gamma = 0 dB$. Furthermore, it can be seen that ADCs with higher resolution should be

TABLE II

THE CHOICE OF QUANTIZATION BITS FOR DIFFERENT κ AND SNR

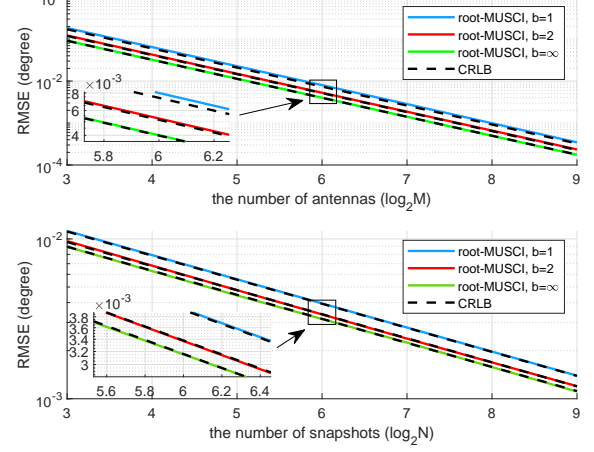
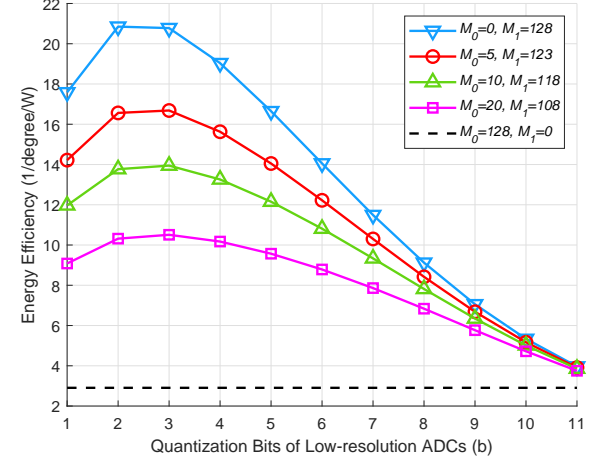
κ	-15 dB	0 dB	15 dB
$0 \sim 0.1$	2	$2 \sim 3$	4
$0.1 \sim 0.8$	$1 \sim 2$	$2 \sim 3$	$3 \sim 4$
$0.8 \sim 1$	1	1	$1 \sim 3$

Fig. 4. RMSE over the SNR using root-MUSIC with $\kappa = 1/2$ and different b .

chosen at $\gamma = 15\text{dB}$. Finally, all analysis and conclusion are summarized in TABLE II for reference. Of course, in some special cases, more or less quantization bit of low-resolution ADCs should be chosen to meet the practical requirement.

Fig. 4 plots curves of RMSE using root-MUSIC method versus SNR for different b with CRLB as a performance benchmark, where $\kappa = 1/2$. Observing Fig. 4, it is clear that root-MUSIC can achieve the associated CRLB. That proves that root-MUSIC can be applied for DOA estimation in mixed-ADC structure without modification. The RMSE difference between $b = 4$ and $b = \infty$ is very small. It proves that mixed-ADC structure can achieve the approximate performance in DOA estimation. And, an insightful observation is that the values of RMSE for all different quantization bits are similar at low SNR. But, the gaps become large as the SNR increases. So, we can conclude that the performance loss of DOA estimation, following the analysis in (26), will increase as the SNR increases in practical application. This is true, because the quantization noise will increase as the SNR increases. Moreover, the curves of RMSE and CRLB are separate when $\gamma = 10\text{ dB}$, which reveals that the AQNM has error at high SNR.

Fig. 5 presents the RMSE of root-MUSIC versus the number of antennas M and the number of snapshots N . Without loss of generality, we assume that $\kappa = 1/4$, $\gamma = 0\text{dB}$, $b = 1, 2, \infty$, $M \in \{8, 32, 128, 512\}$ and $N \in \{16, 64, 256, 1024\}$. All curves of RMSE can attain the corresponding CRLB. Thus, the root-MUSIC is useful for all cases of M and N . The gaps

Fig. 5. RMSE over the number of antennas M and the number of snapshots N using root-MUSIC with $\kappa = 1/4$ and different b .Fig. 6. Energy Efficiency over the quantization bits of low-resolution ADCs with different M_0 and M_1 .

between curve of different b are constant. This is true, because performance loss is not related to the number of antennas and snapshots in (26). With all results, it is clear that, root-MUSIC can be adopted in mixed-ADC structure without modification in all cases. And, we can attain a considerable performance by using the mixed-ADC architecture.

The energy efficiency of DOA estimation for mixed-ADC massive MIMO systems against the quantization bits is shown in Fig. 6. In our numerical examples, we adopt the classic values in massive MIMO systems: $P_{syc} = 50.0\text{ mW}$, $P_{LNA} = 20\text{ mW}$, $P_{mix} = 30.3\text{ mW}$, $P_{fil} = 2.5\text{ mW}$, $P_{IFA} = 3\text{ mW}$, $P_{AGC} = 2\text{ mW}$, $V_{dd} = 3\text{ V}$, $L_{min} = 0.5\text{ }\mu\text{m}$, $f_{cor} = 1\text{ MHz}$ and $B = 20\text{ MHz}$ as in [38], [44] and [45]. 12-bits is chosen as the quantization bit of high-resolution ADCs. Obviously, adopting all low-resolution ADCs attains the best energy efficiency, which reaches the peak when $b = 2$. And, the energy efficiency decreases as the number of high-resolution ADCs increases. However, the achievable rate and spectral efficiency of pure low-resolution ADC architecture are much

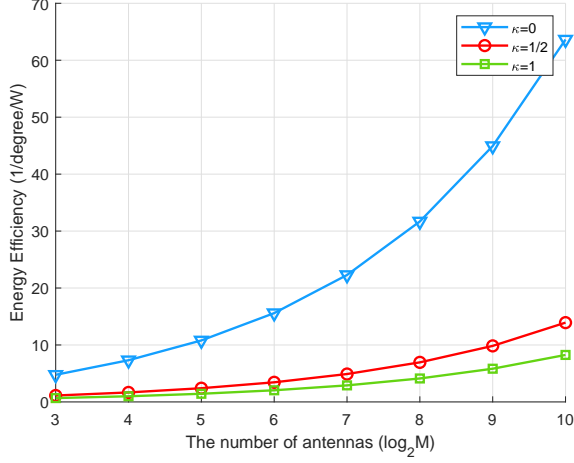


Fig. 7. Energy efficiency over the number of antenna elements M with different proportions of high-resolution ADCs κ .

lower than that of mixed-ADC architecture [38]. Moreover, the accuracy of DOA estimation is so low in low-resolution ADC architecture that mixed-ADC architecture is more likely to be used in practical application. Furthermore, the peaks of curves will move to right as the number of high-resolution ADCs increases. So, we had better adopt more number of quantization bits as low-resolution ADCs increases. That is similar to the analysis in Fig. 3. In practical applications, 2-3 bits of low-resolution ADCs can bring maximum energy efficiency.

In Fig. 7, the energy efficiency over the number of antenna elements is illustrated. The number of antennas M ranges from 8 to 1024. And, the proportions of the number of high-resolution ADCs κ in the mixed-ADC architecture are considered as three different values: $\kappa = 0, 1/2, 1$. As can be seen, all curves increase as the number of antennas M increases. This implies that the mixed-ADC structure has higher energy efficiency for large scale antenna array. Similar to Fig. 6, the low-resolution ADC structure has the highest energy efficiency. However, that is hard to be used due to its low performance of DOA estimation and achievable rate. This means that DOA estimation of massive MIMO systems with mixed-ADCs are very useful in the future applications with large scale antenna arrays.

Fig. 8 shows the trade-off between power consumption and CRLB of mixed-ADC architectures for different quantization bits. Four different cases of κ are shown. Obviously, the massive MIMO with mixed-ADCs consume more power than the one with pure low-resolution ADCs. However, the mixed-ADC structure has more increase in performance for small quantization bits. In addition, the difference of power consumption decreases as b increases. Moreover, the mixed-ADC architecture has a significant improvement in accuracy with little increase in power consumption as the number of quantization bits increases from 1 to 3 or 4, especially when κ is small. However, that has a negligible decrease in CRLB with huge increase in power consumption when $b > 4$. Therefore, to achieve a better trade-off in mixed-ADC structure, the

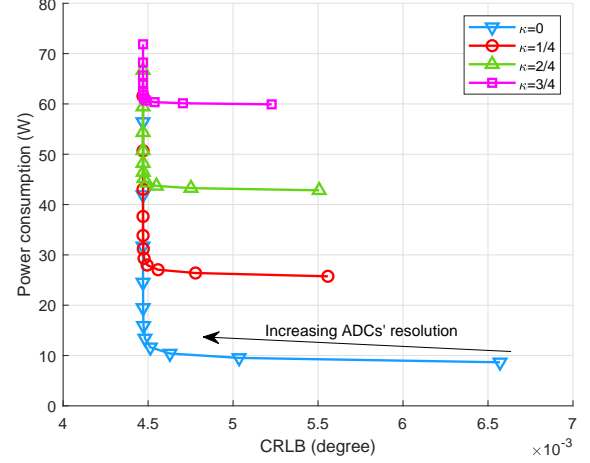


Fig. 8. Trade-off between power consumption and CRLB with different proportions of high-resolution ADCs κ for $\gamma = 0dB$

quantization bits we adopt should be less than 5.

VII. CONCLUSION

In this paper, we built the DOA estimation for the ULA with mixed-ADC. Then, we proved that the root-MUSIC can be applied for this system without modification. Furthermore, we derived the CRLB as the benchmark of the performance. Based on that, the performance loss was investigated, which showed that the mixed-ADC massive MIMO can attain a considerable performance. In addition, the optimal energy efficiency can be achieved in ordinary massive MIMO systems with mixed-ADC when we adopt 1-4 bits of low-resolution ADCs. Finally, we concluded that the mixed-ADC structure can achieve a satisfactory performance of DOA estimation with less circuit cost and power consumption. And, that can be applied to several future practical application scenarios including the 6th generation wireless systems (6G), unmanned aerial vehicle (UAV) communications, internet of things (IOT) and so on.

APPENDIX DERIVATION OF CRLB FOR FULL DIGITAL STRUCTURE WITH MIXED-ADC

In this section, we derive the CRLB for the massive MIMO with mixed-ADCs. In accordance with [1], the corresponding Fisher information matrix (FIM) \mathbf{F} can be written as

$$\mathbf{F} = \text{Tr} \left\{ \mathbf{R}_y^{-1} \frac{\partial \mathbf{R}_y}{\partial \theta_0} \mathbf{R}_y^{-1} \frac{\partial \mathbf{R}_y}{\partial \theta_0} \right\}. \quad (32)$$

Given K independent measurements, the CRLB is given by

$$\text{CRLB} = \frac{1}{K} \mathbf{F}^{-1}. \quad (33)$$

For convenient derivation, $s(n)$, $\mathbf{y}(k)$, $\mathbf{a}(\theta_0)$ and $\mathbf{w}(k)$ are abbreviated as s , \mathbf{y} , \mathbf{a} and \mathbf{w} respectively in the following part. Now, to simplify the derivation, we reformulate \mathbf{y} as

$$\mathbf{y} = \mathbf{T} \mathbf{a} s + \mathbf{T} \mathbf{w} + \mathbf{q}, \quad (34)$$

where

$$\mathbf{T} = \begin{bmatrix} \mathbf{I}_{M_0} & \mathbf{0}_{M_0 \times M_1} \\ \mathbf{0}_{M_1 \times M_0} & \alpha \mathbf{I}_{M_1} \end{bmatrix} \quad (35)$$

and

$$\mathbf{q} = \begin{bmatrix} \mathbf{0}_{M_0 \times 1} \\ \mathbf{w}_F \end{bmatrix}. \quad (36)$$

Then, the \mathbf{R}_y is given by

$$\mathbf{R}_y = \mathbb{E}[\mathbf{y}\mathbf{y}^H] = \gamma \mathbf{T} \mathbf{a} \mathbf{a}^H \mathbf{T}^H + \mathbf{Q}, \quad (37)$$

where

$$\mathbf{Q} = \begin{bmatrix} \mathbf{I}_{M_0} & \mathbf{0}_{M_0 \times M_1} \\ \mathbf{0}_{M_1 \times M_0} & [\alpha^2 + \alpha\beta(\sigma_s^2 + 1)] \mathbf{I}_{M_1} \end{bmatrix}. \quad (38)$$

Thus,

$$\frac{\partial \mathbf{R}_y}{\partial \theta_0} = \gamma \mathbf{T} (\dot{\mathbf{a}} \mathbf{a}^H + \mathbf{a} \dot{\mathbf{a}}^H) \mathbf{T}^H, \quad (39)$$

where $\dot{\mathbf{a}}$ is the differential of \mathbf{a} to θ_0 , which is derived as

$$\dot{\mathbf{a}} = \frac{d}{d\theta_0} \mathbf{a}(\theta_0) = j \frac{2\pi}{\lambda} \cos \theta_0 \mathbf{D} \mathbf{a}, \quad (40)$$

where

$$\mathbf{D} = \begin{bmatrix} d_1 & 0 & \cdots & 0 \\ 0 & d_2 & \cdots & 0 \\ \vdots & \vdots & \ddots & \vdots \\ 0 & 0 & \cdots & d_M \end{bmatrix}. \quad (41)$$

Therefor, with the help of some properties of the trace in [47], FIM can be expressed as

$$\begin{aligned} \mathbf{F} &= \gamma^2 \text{Tr} \{ \mathbf{R}_y^{-1} \mathbf{T} (\dot{\mathbf{a}} \mathbf{a}^H + \mathbf{a} \dot{\mathbf{a}}^H) \mathbf{T}^H \mathbf{R}_y^{-1} \mathbf{T} (\dot{\mathbf{a}} \mathbf{a}^H + \mathbf{a} \dot{\mathbf{a}}^H) \\ &\quad \times \mathbf{T}^H \} \\ &= \gamma^2 (F_a + 2F_b + F_c) \end{aligned} \quad (42)$$

where

$$F_a = (\mathbf{a}^H \mathbf{T}^H \mathbf{R}_y^{-1} \mathbf{T} \dot{\mathbf{a}})^2, \quad (43)$$

$$F_b = (\mathbf{a}^H \mathbf{T}^H \mathbf{R}_y^{-1} \mathbf{T} \dot{\mathbf{a}}) (\dot{\mathbf{a}}^H \mathbf{T}^H \mathbf{R}_y^{-1} \mathbf{T} \dot{\mathbf{a}}), \quad (44)$$

and

$$F_c = (\dot{\mathbf{a}}^H \mathbf{T}^H \mathbf{R}_y^{-1} \mathbf{T} \dot{\mathbf{a}})^2. \quad (45)$$

In the following, resorting to the well-known Sherman-Morrison-Woodbury formula in [48],

$$(A + XRY)^{-1} = A^{-1} - A^{-1}X(R^{-1} + YA^{-1}X)^{-1}YA^{-1}, \quad (46)$$

we can get

$$\mathbf{R}_y^{-1} = \mathbf{Q}^{-1} - \frac{\mathbf{Q}^{-1} \mathbf{T} \mathbf{a} \mathbf{a}^H \mathbf{T}^H \mathbf{Q}^{-1}}{\gamma^{-1} + \mathbf{a}^H \mathbf{T}^H \mathbf{Q}^{-1} \mathbf{T} \mathbf{a}}. \quad (47)$$

Let us define

$$\xi = \mathbf{a}^H \mathbf{T}^H \mathbf{Q}^{-1} \mathbf{T} \mathbf{a} = M_0 + \frac{\alpha}{\beta \sigma_s^2 + 1} M_1. \quad (48)$$

Then, we can get

$$\begin{aligned} &\mathbf{a}^H \mathbf{T}^H \mathbf{R}_y^{-1} \mathbf{T} \dot{\mathbf{a}} \\ &= \mathbf{a}^H \mathbf{T}^H \left(\mathbf{Q}^{-1} - \frac{\mathbf{Q}^{-1} \mathbf{T} \mathbf{a} \mathbf{a}^H \mathbf{T}^H \mathbf{Q}^{-1}}{\gamma^{-1} + \xi} \right) \mathbf{T} \dot{\mathbf{a}} \\ &= j \frac{2\pi}{\lambda} \cos \theta_0 \left(1 - \frac{\xi}{\gamma^{-1} + \xi} \right) \\ &\quad \times \left(\sum_{m=1}^{M_0} d_m + \frac{\alpha}{\beta \sigma_s^2 + 1} \sum_{m=M_0+1}^M d_m \right) \\ &= j \frac{2\pi}{\lambda(\gamma\xi + 1)} \cos \theta_0 \mu, \end{aligned} \quad (49)$$

where

$$\mu = \sum_{m=1}^{M_0} d_m + \frac{\alpha}{\beta \sigma_s^2 + 1} \sum_{m=M_0+1}^M d_m. \quad (50)$$

Accordingly, substituting (49) into (43), F_a can be expressed as

$$\begin{aligned} F_a &= (\mathbf{a}^H \mathbf{T}^H \mathbf{R}_y^{-1} \mathbf{T} \dot{\mathbf{a}})^2 \\ &= -\frac{4\pi^2}{\lambda^2(\gamma\xi + 1)^2} \cos^2 \theta_0 \mu^2. \end{aligned} \quad (51)$$

Similar to the derivation of F_a , $\dot{\mathbf{a}}^H \mathbf{T}^H \mathbf{R}_y^{-1} \mathbf{T} \dot{\mathbf{a}}$ can be derived as follows,

$$\begin{aligned} &\dot{\mathbf{a}}^H \mathbf{T}^H \mathbf{R}_y^{-1} \mathbf{T} \dot{\mathbf{a}} \\ &= \dot{\mathbf{a}}^H \mathbf{T}^H \left(\mathbf{Q}^{-1} - \frac{\mathbf{Q}^{-1} \mathbf{T} \mathbf{a} \mathbf{a}^H \mathbf{T}^H \mathbf{Q}^{-1}}{\gamma^{-1} + \xi} \right) \mathbf{T} \dot{\mathbf{a}} \\ &= -j \frac{2\pi}{\lambda(\gamma\xi + 1)} \cos \theta_0 \mu. \end{aligned} \quad (52)$$

Thus, F_c can be given by

$$\begin{aligned} F_c &= (\dot{\mathbf{a}}^H \mathbf{T}^H \mathbf{R}_y^{-1} \mathbf{T} \dot{\mathbf{a}})^2 = F_a \\ &= -\frac{4\pi^2}{\lambda^2(\gamma\xi + 1)^2} \cos^2 \theta_0 \mu^2. \end{aligned} \quad (53)$$

Now, let us focus on the derivation of F_b . The first part of (44) can be given by

$$\begin{aligned} &\mathbf{a}^H \mathbf{T}^H \mathbf{R}_y^{-1} \mathbf{T} \dot{\mathbf{a}} \\ &= \mathbf{a}^H \mathbf{T}^H \left(\mathbf{Q}^{-1} - \frac{\mathbf{Q}^{-1} \mathbf{T} \mathbf{a} \mathbf{a}^H \mathbf{T}^H \mathbf{Q}^{-1}}{\gamma^{-1} + \xi} \right) \mathbf{T} \dot{\mathbf{a}} \\ &= \xi \left(1 - \frac{\xi}{\gamma^{-1} + \xi} \right) \\ &= \frac{\xi}{\gamma\xi + 1}. \end{aligned} \quad (54)$$

And, the second part is expressed as

$$\begin{aligned}
& \dot{\mathbf{a}}^H \mathbf{T}^H \mathbf{R}_y^{-1} \mathbf{T} \dot{\mathbf{a}} \\
&= \dot{\mathbf{a}}^H \mathbf{T}^H \left(\mathbf{Q}^{-1} - \frac{\mathbf{Q}^{-1} \mathbf{T} \mathbf{a} \mathbf{a}^H \mathbf{T}^H \mathbf{Q}^{-1}}{\gamma^{-1} + \xi} \right) \mathbf{T} \dot{\mathbf{a}} \\
&= \frac{4\pi^2}{\lambda^2} \cos^2 \theta_0 \left[\left(\sum_{m=1}^{M_0} d_m^2 + \frac{\alpha}{\beta \sigma_s^2 + 1} \right. \right. \\
&\quad \times \sum_{m=M_0+1}^M d_m^2 \left. \right) - \frac{1}{\gamma^{-1} + \xi} \left(\sum_{m=1}^{M_0} d_m \right. \\
&\quad \left. \left. + \frac{\alpha}{\beta \sigma_s^2 + 1} \sum_{m=M_0+1}^M d_m \right) \right]^2 \\
&= \frac{4\pi^2}{\lambda^2} \cos^2 \theta_0 \left(\nu - \frac{\gamma \mu^2}{\gamma \xi + 1} \right), \tag{55}
\end{aligned}$$

where

$$\nu = \sum_{m=1}^{M_0} d_m^2 + \frac{\alpha}{\beta \sigma_s^2 + 1} \sum_{m=M_0+1}^M d_m^2. \tag{56}$$

Combining (54) and (55), F_b in (44) is represented by

$$\begin{aligned}
F_b &= (\mathbf{a}^H \mathbf{T}^H \mathbf{R}_y^{-1} \mathbf{T} \mathbf{a}) (\dot{\mathbf{a}}^H \mathbf{T}^H \mathbf{R}_y^{-1} \mathbf{T} \dot{\mathbf{a}}) \\
&= \frac{4\pi^2 \xi}{\lambda^2 (\gamma \xi + 1)} \cos^2 \theta_0 \left(\nu - \frac{\gamma \mu^2}{\gamma \xi + 1} \right) \tag{57}
\end{aligned}$$

Finally, substitute F_a in (51), F_b in (57) and F_c in (53) into (42), which yields

$$\begin{aligned}
\mathbf{F} &= \gamma^2 (F_a + 2F_b + F_c) \\
&= \frac{8\pi^2 \gamma^2}{\lambda^2 (\gamma \xi + 1)} \cos^2 \theta_0 (\xi \nu - \mu^2). \tag{58}
\end{aligned}$$

Therefore, the CRLB is given by

$$\begin{aligned}
CRLB &= \frac{1}{K} \mathbf{F}^{-1} \\
&= \frac{\lambda^2 (\gamma \xi + 1)}{8K \pi^2 \gamma^2 \cos^2 \theta_0 (\xi \nu - \mu^2)}. \tag{59}
\end{aligned}$$

The derivation of CRLB for the massive MIMO system with mixed-ADCs is completed. \blacksquare

REFERENCES

- [1] T. E. Tuncer and B. Friedlander, *Classical and Modern Direction-of-Arrival Estimation*. Academic Press, 2009.
- [2] Y. Li, F. Shu, B. Shi, X. Cheng, Y. Song, and J. Wang, "Enhanced RSS-based UAV localization via trajectory and multi-base stations," *IEEE Commun. Lett.*, pp. 1–1, 2021.
- [3] F. Shu, S. Yang, J. Lu, and J. Li, "On impact of earth constraint on TDOA-based localization performance in passive multisatellite localization systems," *IEEE Systems Journal*, vol. 12, no. 4, pp. 3861–3864, 2018.
- [4] Y. Zeng and R. Zhang, "Energy-efficient UAV communication with trajectory optimization," *IEEE Trans. Wireless Commun.*, vol. 16, no. 6, pp. 3747–3760, 2017.
- [5] S. Hong, C. Pan, H. Ren, K. Wang, and A. Nallanathan, "Artificial-noise-aided secure MIMO wireless communications via intelligent reflecting surface," *IEEE Trans. Commun.*, vol. 68, no. 12, pp. 7851–7866, 2020.
- [6] Q. Wu and R. Zhang, "Beamforming optimization for wireless network aided by intelligent reflecting surface with discrete phase shifts," *IEEE Trans. Commun.*, vol. 68, no. 3, pp. 1838–1851, 2020.
- [7] C. Pan, H. Ren, K. Wang, W. Xu, M. Elkashlan, A. Nallanathan, and L. Hanzo, "Multicell MIMO communications relying on intelligent reflecting surfaces," *IEEE Trans. Wireless Commun.*, vol. 19, no. 8, pp. 5218–5233, 2020.
- [8] J. Hu, F. Shu, and J. Li, "Robust synthesis method for secure directional modulation with imperfect direction angle," *IEEE Commun. Lett.*, vol. 20, no. 6, pp. 1084–1087, 2016.
- [9] Z. Lu, L. Sun, S. Zhang, X. Zhou, J. Lin, W. Cai, J. Wang, J. Lu, and F. Shu, "Optimal power allocation for secure directional modulation networks with a full-duplex UAV user," *Science China (Information Sciences)*, vol. v.62, no. 08, pp. 44–55, 2019.
- [10] X. Zhou, J. Li, F. Shu, Q. Wu, Y. Wu, W. Chen, and L. Hanzo, "Secure swiフト for directional modulation-aided AF relaying networks," *IEEE J. Sel. Areas Commun.*, vol. 37, no. 2, pp. 253–268, 2019.
- [11] F. Shu, T. Shen, L. Xu, Y. Qin, S. Wan, S. Jin, X. You, and J. Wang, "Directional modulation: A physical-layer security solution to 5G and future wireless networks," *IEEE Network*, vol. 34, no. 2, pp. 210–216, 2020.
- [12] J. Hu, S. Yan, F. Shu, J. Wang, J. Li, and Y. Zhang, "Artificial-noise-aided secure transmission with directional modulation based on random frequency diverse arrays," *IEEE Access*, vol. 5, pp. 1658–1667, 2017.
- [13] T. Shen, S. Zhang, R. Chen, J. Wang, J. Hu, F. Shu, and J. Wang, "Two practical random-subcarrier-selection methods for secure precise wireless transmissions," *IEEE Trans. Veh. Technol.*, vol. 68, no. 9, pp. 9018–9028, 2019.
- [14] F. Shu, X. Wu, J. Hu, J. Li, R. Chen, and J. Wang, "Secure and precise wireless transmission for random-subcarrier-selection-based directional modulation transmit antenna array," *IEEE J. Sel. Areas Commun.*, vol. 36, no. 4, pp. 890–904, 2018.
- [15] N. Kaur and S. K. Sood, "An energy-efficient architecture for the internet of things (IoT)," *IEEE Systems Journal*, vol. 11, no. 2, pp. 796–805, 2017.
- [16] R. Schmidt, "A signal subspace approach to multiple emitter location and spectral estimation," *Ph. D. Dissertation. Stanford Univ.*, 1981.
- [17] R. Roy, A. Paulraj, and T. Kailath, "ESPRIT—a subspace rotation approach to estimation of parameters of coids in noise," *IEEE Transactions on Acoustics, Speech, and Signal Processing*, vol. 34, no. 5, pp. 1340–1342, 1986.
- [18] A. Barabell, "Improving the resolution performance of eigenstructure-based direction-finding algorithms," in *ICASSP '83. IEEE International Conference on Acoustics, Speech, and Signal Processing*, vol. 8, 1983, pp. 336–339.
- [19] M. Pesavento, A. B. Gershman, and M. Haardt, "Unitary root-MUSIC with a real-valued eigendecomposition: a theoretical and experimental performance study," *IEEE Trans. Signal Process.*, vol. 48, no. 5, pp. 1306–1314, 2000.
- [20] F. Yan, M. Jin, S. Liu, and X. Qiao, "Real-valued MUSIC for efficient direction estimation with arbitrary array geometries," *IEEE Trans. Signal Process.*, vol. 62, no. 6, pp. 1548–1560, 2014.
- [21] L. Cheng, Y. Wu, J. Zhang, and L. Liu, "Subspace identification for DOA estimation in massive/full-dimension MIMO systems: Bad data mitigation and automatic source enumeration," *IEEE Trans. Signal Process.*, vol. 63, no. 22, pp. 5897–5909, 2015.
- [22] D. Fan, F. Gao, Y. Liu, Y. Deng, G. Wang, Z. Zhong, and A. Nallanathan, "Angle domain channel estimation in hybrid millimeter wave massive MIMO systems," *IEEE Trans. Wireless Commun.*, vol. 17, no. 12, pp. 8165–8179, 2018.
- [23] F. Shu, Y. Qin, T. Liu, L. Gui, Y. Zhang, J. Li, and Z. Han, "Low-complexity and high-resolution DOA estimation for hybrid analog and digital massive MIMO receive array," *IEEE Trans. Commun.*, vol. 66, no. 6, pp. 2487–2501, 2018.
- [24] K. Wu, W. Ni, T. Su, R. P. Liu, and Y. J. Guo, "Robust unambiguous estimation of angle-of-arrival in hybrid array with localized analog subarrays," *IEEE Trans. Wireless Commun.*, vol. 17, no. 5, pp. 2987–3002, 2018.
- [25] H. Huang, J. Yang, H. Huang, Y. Song, and G. Gui, "Deep learning for super-resolution channel estimation and DOA estimation based massive MIMO system," *IEEE Trans. Veh. Technol.*, vol. 67, no. 9, pp. 8549–8560, 2018.
- [26] D. Hu, Y. Zhang, L. He, and J. Wu, "Low-complexity deep-learning-based DOA estimation for hybrid massive MIMO systems with uniform circular arrays," *IEEE Wireless Commun. Lett.*, vol. 9, no. 1, pp. 83–86, 2020.
- [27] X. Huang and B. Liao, "One-bit MUSIC," *IEEE Signal Process. Lett.*, vol. 26, no. 7, pp. 961–965, 2019.
- [28] B. Shi, N. Chen, X. Zhu, Y. Qian, Y. Zhang, F. Shu, and J. Wang, "Impact of low-resolution ADC on DOA estimation performance for massive MIMO receive array," *arXiv preprint*, vol. arXiv:2011.00451, 2020.

- [29] H. Lee and C. G. Sodini, "Analog-to-digital converters: Digitizing the analog world," *Proceedings of the IEEE*, vol. 96, no. 2, pp. 323–334, 2008.
- [30] J. Singh, O. Dabeer, and U. Madhow, "On the limits of communication with low-precision analog-to-digital conversion at the receiver," *IEEE Trans. Commun.*, vol. 57, no. 12, pp. 3629–3639, 2009.
- [31] L. Fan, S. Jin, C. Wen, and H. Zhang, "Uplink achievable rate for massive MIMO systems with low-resolution ADC," *IEEE Commun. Lett.*, vol. 19, no. 12, pp. 2186–2189, 2015.
- [32] S. Jin, X. Liang, K. Wong, X. Gao, and Q. Zhu, "Ergodic rate analysis for multipair massive MIMO two-way relay networks," *IEEE Trans. Wireless Commun.*, vol. 14, no. 3, pp. 1480–1491, 2015.
- [33] C. Kong, C. Zhong, S. Jin, S. Yang, H. Lin, and Z. Zhang, "Full-duplex massive MIMO relaying systems with low-resolution ADCs," *IEEE Trans. Wireless Commun.*, vol. 16, no. 8, pp. 5033–5047, 2017.
- [34] P. Dong, H. Zhang, W. Xu, and X. You, "Efficient low-resolution ADC relaying for multiuser massive MIMO system," *IEEE Trans. Veh. Technol.*, vol. 66, no. 12, pp. 11 039–11 056, 2017.
- [35] L. Xu, L. Sun, G. Xia, T. Liu, F. Shu, Y. Zhang, and J. Wang, "Secure hybrid digital and analog precoder for mmWave systems with low-resolution DACs and finite-quantized phase shifters," *IEEE Access*, vol. 7, pp. 109 763–109 775, 2019.
- [36] W. Tan, S. Jin, C. Wen, and Y. Jing, "Spectral efficiency of mixed-ADC receivers for massive MIMO systems," *IEEE Access*, vol. 4, pp. 7841–7846, 2016.
- [37] J. Zhang, L. Dai, Z. He, S. Jin, and X. Li, "Performance analysis of mixed-ADC massive MIMO systems over rician fading channels," *IEEE J. Sel. Areas Commun.*, vol. 35, no. 6, pp. 1327–1338, 2017.
- [38] J. Zhang, L. Dai, Z. He, B. Ai, and O. A. Dobre, "Mixed-ADC/DAC multipair massive MIMO relaying systems: Performance analysis and power optimization," *IEEE Trans. Commun.*, vol. 67, no. 1, pp. 140–153, 2019.
- [39] N. Liang and W. Zhang, "Mixed-ADC massive MIMO," *IEEE J. Sel. Areas Commun.*, vol. 34, no. 4, pp. 983–997, 2016.
- [40] T. Zhang, C. Wen, S. Jin, and T. Jiang, "Mixed-ADC massive MIMO detectors: Performance analysis and design optimization," *IEEE Trans. Wireless Commun.*, vol. 15, no. 11, pp. 7738–7752, 2016.
- [41] O. Orhan, E. Erkip, and S. Rangan, "Low power analog-to-digital conversion in millimeter wave systems: Impact of resolution and bandwidth on performance," in *2015 Information Theory and Applications Workshop (ITA)*, 2015, pp. 191–198.
- [42] J. Zhu, C. Wen, J. Tong, C. Xu, and S. Jin, "Grid-less variational bayesian channel estimation for antenna array systems with low resolution ADCs," *IEEE Trans. Wireless Commun.*, vol. 19, no. 3, pp. 1549–1562, 2020.
- [43] J. Mo, A. Alkhateeb, S. Abu-Surra, and R. W. Heath, "Hybrid architectures with few-bit ADC receivers: Achievable rates and energy-rate tradeoffs," *IEEE Trans. Wireless Commun.*, vol. 16, no. 4, pp. 2274–2287, 2017.
- [44] C. He, B. Sheng, P. Zhu, and X. You, "Energy efficient comparison between distributed MIMO and co-located MIMO in the uplink cellular systems," in *2012 IEEE Vehicular Technology Conference (VTC Fall)*, 2012, pp. 1–5.
- [45] Shuguang Cui, A. J. Goldsmith, and A. Bahai, "Energy-constrained modulation optimization," *IEEE Trans. Wireless Commun.*, vol. 4, no. 5, pp. 2349–2360, 2005.
- [46] E. Lauwers and G. Gielen, "Power estimation methods for analog circuits for architectural exploration of integrated systems," *IEEE Trans. Very Large Scale Integr. (VLSI) Syst.*, vol. 10, no. 2, pp. 155–162, 2002.
- [47] X. Zhang, *Matrix analysis and applications*. Cambridge University Press, 2017.
- [48] R. A. Horn and C. R. Johnson, *Matrix Analysis*. Cambridge University Press, 2012.